Dyes and Pigments 122 (2015) 246–256

Contents lists available at ScienceDirect

Dyes and Pigments

journal homepage: www.elsevier.com/locate/dyepig

Zero-, one-, two- and three-dimensional coordination polymers based on tetracarboxylic acid: Syntheses, structures, magnetic and luminescent properties

Li-rong Yang*, Liu Liu, Chen Lian, Meng-yan Liu, Zhen-huan Xu, Li-Ce Wang, Xu Guo, Yin-shuang Long

Henan Key Laboratory of Polyoxometalate, Institute of Molecule and Crystal Engineering, College of Chemistry and Chemical Engineering, Henan University, Kaifeng 475004, PR China

ARTICLE INFO

Article history:
Received 29 April 2015
Received in revised form
14 June 2015
Accepted 30 June 2015
Available online 9 July 2015

Keywords:
Tetracarboxylic acid
Coordination polymer
Magnetic properties
Luminescent properties
Metal-organic frameworks
Intermolecular forces

ABSTRACT

A series of coordination polymers, namely, $\{[Co(H_2ttac)(phen)_2]\cdot 4H_2O\}_n$ (**1**), $\{[Zn(H_2ttac)(phen)_2]\cdot 4H_2O\}_n$ (**2**), $[Cu(H_2ttac)(phen)]_n$ (**3**), $[Zn_2(ttac)(DMZ)H_2O]_n$ (**4**), and $[Cd(ttac)(phen)H_2O]_n$ (**5**)(H_4ttac = 4,5-di(3'-carboxylphenyl)-phthalic acid, phen = 1,10-phenanthroline, DMZ = Dimidazole) have been prepared under hydrothermal conditions and characterized by elemental analysis, IR spectroscopy, and single crystal X-ray diffraction. Structural analysis reveals that the as-synthesized coordination polymers have different structures, ranging from zero-(**1** and **2**), one-(**3**), two-(**4**) to three-(**5**) dimensions, which are mainly due to the different metal ions, the degree of deprotonation and coordination modes of the H_4ttac ligands. It is worth mentioning that, based on the diversified $\pi-\pi$ stacking and/or C–H$\cdots\pi$ interactions between H_4ttac ligands and/or nitrogen-containing auxiliary ligands, **1**–**4** are assembled form low-dimensional structures into three-dimensional (3D) frameworks. Especially, Jahn-Teller effect occurs in **3** and its magnetic study confirms that it presents antiferromagnetic coupling through the $(O_2C\text{-}Ar\text{-}Ar\text{-}CO_2)_2$ bridges. Significantly, luminescent emission of **3** displays selective recognition towards L-Arginin. Thermogravimetric (TG) analyses of the coordination polymers have also been investigated.

1. Introduction

As well as we know, the design and syntheses of coordination polymers (CPs) has been attracting enormous interest of synthetic chemists not only due to their networks made up of organic linkers and metal cations, often forming diversity of architectures and fascinating topologies, but also for their potentially industrial applications in gas storage and separation, heterogeneous catalysis, drug delivery, magnetic properties, molecular recognition and selective luminescent probes and so on [1–14].

Obviously, coordination mode of organic linkers and the geometry of metal cations have a major impact on the topological structures of the coordination polymers. Usually, multi-dentate organic ligands like multi-carboxylic acids are recommended to polymerize into extended open frameworks, because these ligands may potentially provide various coordination modes and favor the construction of multi-dimensional coordination polymers [15–23]. The transition metal (TM) ions such as Co(II), Cu(II), Zn(II), and Cd(II) have been used in structure coordination polymers on account of specific geometry and excellent chemical properties [24–31]. In the meantime, nitrogen-containing auxiliary ligands containing pyridine and imidazole rings are superior in terms of hydrogen-bonding formation and $\pi-\pi$ stacking interactions that are significant for affording extended open frameworks *via* polymerization [32–35]. Furthermore, the reaction conditions such as pH value, temperature, reaction time, and material ratio, etc, can be utilized to adjust and functionalize the preassembled structures of coordination polymers.

In the assembling strategies of the coordination polymers, aromatic–aromatic or $\pi-\pi$ stacking as well as C–H$\cdots\pi$ interactions are important non-covalent intermolecular forces and may play a role in the connection process of the frameworks. Better understanding and utilizing, these intermolecular forces are of fundamental significance for the further development of arrangement

* Corresponding author.
E-mail addresses: lirongyang@henu.edu.cn, lirongyang@163.com (L.-r. Yang).

http://dx.doi.org/10.1016/j.dyepig.2015.06.035
0143-7208/

and tuning of high-dimensional crystal structures, especially when strong hydrogen bonds are absent. Nitrogen-containing in the aromatic rings may show preferences of crystal structures with stacking. Heteroatoms in an aromatic system induce differentiation of π (and σ) electron distributions. As is well-known, nitrogen-containing aromatic rings show smaller stacking separation because the van der Waals radius for nitrogen is smaller than that for carbon atom. In the present work, nitrogen-containing ligand such as phenanthroline and dimidazole were chosen as the auxiliary ligands together with a flexible tetrahydric acid to construct a series of complexes utilizing the diversified $\pi-\pi$ stacking and C–H$\cdots\pi$ interactions [36–38].

Hydro(solvo)thermal synthesis has been proven to be an effective method in preparing functional coordination polymers and growing single crystals for structural studies. Taking into account the geometry and its degree of protonation of the title multicarboxylic acid, as well as the flexibility of carboxy groups, different coordination conformations of the ligand may occur due to its coordination versatility and capability to build various secondary building units (SBUs). Furthermore, the introduction of nitrogen-containing co-linkers is beneficial to the fabrication of different dimensionalities of the coordination polymers. In this report, we selected a flexible tetracarboxylic acid, namely, 4,5-di(3'-carboxylphenyl)-phthalic acid (H_4ttac), a symmetric multidentate ligand, together with different metal centers by adjusting pH value, temperature, and auxiliary ligands, then, five coordination polymers have been prepared successfully, $\{[Co(H_2ttac)(phen)_2]\cdot 4H_2O\}_n$ (**1**), $\{[Zn(H_2ttac)(phen)_2]\cdot 4H_2O\}_n$ (**2**), $[Cu(H_2ttac)(phen)]_n$ (**3**), $[Zn_2(ttac)(DMZ)H_2O]_n$ (**4**), and $[Cd(ttac)(phen)H_2O]_n$ (**5**), the synthetic route is shown in Scheme 1. Peculiarly, there are four coordination modes in the coordination polymers **1**–**5**, detailed information are illustrated in Scheme 2.

2. Experimental section

2.1. Materials and physical measurements

All chemicals were commercially purchased and used without further purification. Elemental analyses (C, H, and N) were performed with a Perkin–Elmer 240 CHN Elemental Analyzer. IR spectra in the range of 400–4000 cm^{-1} were recorded with an AVATAR 360 FT-IR spectrometer (KBr pellets were used). The crystal structure was determined with a Bruker Smart CCD X-ray single-crystal diffractometer. Excitation and emission spectra were obtained with an F-7000 FL spectrofluorometer at room temperature. Thermogravimetric (TG) and differential thermogravimetric (DTG) analyses were conducted with a Perkin–Elmer TGA7 system under flowing N_2 stream (flow rate 40 mL/min) from room temperature to

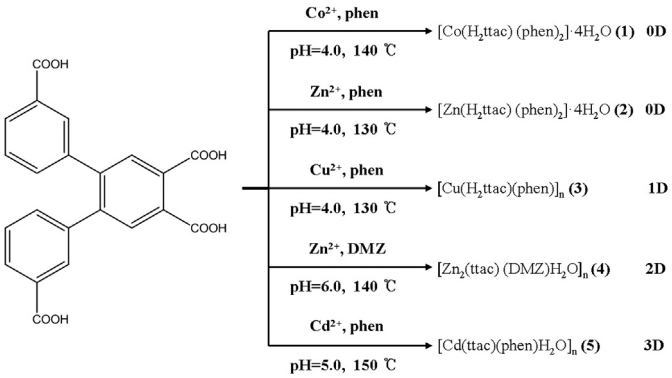

Scheme 1. Experimental routes for coordination polymers **1**–**5**.

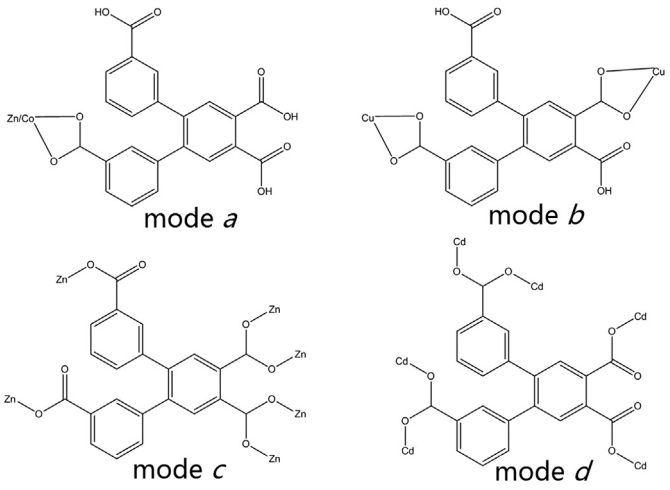

Scheme 2. The coordination modes of H_4ttac ligand in coordination polymers **1**–**5**.

1000 °C at a heating rate of 10 K/min. Powder X-ray diffraction (PXRD) patterns were recorded on a Bruker D8 Advance instrument with Cu-Kα radiation (λ = 1.54056 Å) in the range 2θ = 5–45° at room temperature.

2.2. Synthesis of the coordination polymers ***1*–*5***

2.2.1. Synthesis of $[Co(H_2ttac)(phen)_2]\cdot 4H_2O$ (1)

A mixture of 4,5-di(3'-carboxylphenyl)-phthalic acid (0.05 mmol, 20.3 mg), cobalt perchlorate-hydrate (0.1 mmol, 36.6 mg) and 1,10-phenanthroline (0.1 mmol, 18.0 mg) in 10 mL of water was adjusted to pH 4.0 with 1 mol L^{-1} KOH solution. The mixture was then transferred to and sealed in a 25 mL Teflon-lined stainless autoclave, followed by heating at 140 °C for 72 h to afford pink block-shaped crystals in 24.7% yield after slowly cooling to room temperature at a rate of 5 °C/h. Elemental analysis calculated for $C_{46}H_{36}CoN_4O_{12}$ (895.72): C 62.34%, H 4.17%, N 6.13%; Found: C 61.70%, H 4.05%, N 6.26%. Selected IR (cm^{-1}): 3430(m), 3066(m), 2926(m), 2604(m), 1704(s), 1605(s), 1517(m), 1430(m), 1373(s), 1311(m), 1298(m), 1256(m), 1117(w), 1028(w), 816(m), 765(m), 717(m), 651(m), 560(m).

2.2.2. Synthesis of $[Zn(H_2ttac)(phen)_2]\cdot 4H_2O$ (2)

A mixture of 4,5-di(3'-carboxylphenyl)-phthalic acid (0.05 mmol, 20.3 mg), zinc perchlorate-hydrate (0.1 mmol, 26.4 mg) and 1,10-phenanthroline (0.1 mmol, 18.0 mg) in 10 mL of water was adjusted to pH 4.0 with 1 mol L^{-1} KOH solution. The mixture was then transferred to and sealed in a 25 mL Teflon-lined stainless autoclave, followed by heating at 130 °C for 72 h to afford colorless block-shaped crystals in 35.2% yield after slowly cooling to room temperature at a rate of 5 °C/h. Elemental analysis calculated for $C_{46}H_{36}ZnN_4O_{12}$ (902.16): C 61.77%, H 4.09%, N 6.51%; Found: C 61.24%, H 4.02%, N 6.21%. Selected IR (cm^{-1}): 3427(m), 3066(m), 2927(m), 2607(m), 1704(s), 1582(s), 1520(m), 1430(s), 1398(w), 1361(m), 1299(m), 1256(m), 1149(w), 1110(m), 928(m), 854(s), 814(m), 770(s), 727(s), 650(w), 562(w).

2.2.3. Synthesis of $[Cu(H_2ttac)(phen)]_n$ (3)

A mixture of 4,5-di(3'-carboxylphenyl)-phthalic acid (0.05 mmol, 20.3 mg), copper perchlorate-hydrate (0.1 mmol, 37.1 mg) and 1,10-phenanthroline (0.1 mmol, 18.0 mg) in 10 mL of water was adjusted to pH 4.0 with 1 mol L^{-1} KOH solution. The mixture was then transferred to and sealed in a 25 mL Teflon-lined stainless autoclave, followed by heating at 130 °C for 72 h to afford

sapphirine block-shaped crystals in 86.3% yield after slowly cooling to room temperature at a rate of 5 °C/h. Elemental analysis calculated for $C_{34}H_{20}CuN_2O_8$ (648.06): C 63.69%, H 3.07%, N 4.53%; Found: C 63.01%, H 3.11%, N 4.33%. Selected IR (cm^{-1}): 3431(m), 3065(m), 2924(m), 2854(m), 1707(s), 1625(m), 1566(s), 1520(m), 1488(s), 1488(w), 1427(m), 1394(m), 1212(m), 1166(w), 1113(w), 1083(m), 854(s), 810(m), 771(m), 743(m), 724(m), 700(m), 666(m), 628(m), 564(w), 538(w), 511(w), 484(w).

2.2.4. Synthesis of [Zn_2(ttac)(DMZ)H_2O]n (4)

A mixture of 4,5-di- (3'-carboxylphenyl)-phthalic acid (0.05 mmol, 20.3 mg), zinc perchlorate-hydrate (0.1 mmol, 26.4 mg) and dimidazole (0.1 mmol, 13.4 mg) in 10 mL of water was adjusted to pH 6.0 with 1 mol L^{-1} KOH solution. The mixture was then transferred to and sealed in a 25 mL Teflon-lined stainless autoclave, followed by heating at 140 °C for 72 h to afford colorless block-shaped crystals in 57.9% yield after slowly cooling to room temperature at a rate of 5 °C/h. Elemental analysis calculated for $C_{28}H_{16}Zn_2N_4O_9$ (683.19): C 50.47%, H 3.52%, N 8.59%; Found: C 49.22%, H 3.36%, N 8.20%. Selected IR (cm^{-1}): 3284(m), 3143(m), 2937(m), 1554(s), 1398(s), 1357(m), 1266(w), 1179(w), 1098(m), 1001(w), 910(w), 813(m), 769(s), 698(m), 654(w), 586(w), 555(w), 499(w), 448(w).

2.2.5. Synthesis of [Cd(ttac)(phen)H_2O]$_n$ (5)

A mixture of 4,5-di(3'-carboxylphenyl)-phthalic acid (0.05 mmol, 20.3 mg), cadmium perchlorate-hydrate (0.1 mmol, 41.9 mg) and 1,10-phenanthroline (0.1 mmol, 18.0 mg) in 10 mL of water was adjusted to pH 5.0 with 1 mol L^{-1} KOH solution. The mixture was then transferred to and sealed in a 25 mL Teflon-lined stainless autoclave, followed by heating at 150 °C for 72 h to afford colorless block-shaped crystals in 66.7% yield after slowly cooling to room temperature at a rate of 5 °C/h. Elemental analysis calculated for $C_{23}H_{15}CuN_2O_5$ (511.77): C 52.55%, H 2.74%, N 5.69%; Found: C 53.98%, H 2.95%, N 5.47%. Selected IR (cm^{-1}): 3427(m), 3059(m), 2931(m), 1554(s), 1394(s), 1304(m), 1266(w), 1112(w), 1097(m), 900(w), 854(s), 816(m), 775(s), 727(s), 699(m), 633(w), 568(w), 426(w).

2.3. Crystallographic data collection and refinement

All hydrogen atoms were refined isotropically as a riding mode using the default Single-crystal diffraction data **1**–**5** were collected suitable single crystals of the coordination polymers on a Bruker Smart CCD X-ray single-crystal diffractometer with graphite monochromated MoKα-radiation (λ = 0.71073 Å) at 296(2) K. All independent reflections were collected in a range of 1.30–25.00° for **1**, 1.32 to 25.00 for **2**, 1.75 to 25.00 for **3**, 1.57 to 25.00 for **4**, 1.63 to 24.99 for **5**, (determined in the subsequent refinement). Multi-scan empirical absorption corrections were applied to the data using the SADABS. The crystal structure was solved by direct methods and Fourier synthesis. Positional and thermal parameters were refined by the full-matrix least-squares method on F_2 using the SHELXTL software package. The final least-square cycle of refinement gave, $R_1 = 0.0665$, $wR_2 = 0.1621$ for **1**, $R_1 = 0.0728$, $wR_2 = 0.1685$ for **2**, $R_1 = 0.0391$, $wR_2 = 0.1022$ for **3**, $R_1 = 0.0375$, $wR_2 = 0.1136$ for **4**, $R_1 = 0.0914$, $wR_2 = 0.1718$ for **5**. The weighting scheme, $w = 1/[\sigma^2(F_0^2) + (0.1084P)^2 + 0.00P]$ for **1**, $w = 1/[\sigma^2(F_0^2) + (0.1091P)^2 + 0.00P]$ for **2**, $w = 1/[\sigma^2(F_0^2) + (0.0562P)^2 + 0.13P]$ for **3**, $w = 1/[\sigma^2(F_0^2) + (0.0630P)^2 + 0.00P]$ for **4**, $w = 1/[\sigma^2(F_0^2) + (0.0113P)^2 + 94.21P]$ for **5**, where $P = (F_0^2+2F_c^2)/3$. A summary of the key crystallographic information is given in Table 1. Selected bond lengths and band angles for the coordination polymers **1**–**5** are listed in Table S1. Hydrogen-bond lengths (Å) and angles (°) for **1**–**5** are listed in Table S2.

3. Results and discussion

3.1. X-ray powder diffraction

The powder XRD patterns of coordination polymers **3**, **4**, and **5** have been investigated. As shown in Fig. S1, the experimental powder XRD patterns are consistent with the simulated ones on the basis of the single-crystal structure, which indicated that the corresponding samples are pure.

Table 1
Summary of crystallographic data for coordination polymers **1**–**5**.

	1	2	3	4	5
Formula	$C_{46}H_{36}CoN_4O_{12}$	$C_{46}H_{36}ZnN_4O_{12}$	$C_{34}H_{20}CuN_2O_8$	$C_{28}H_{16}Zn_2N_4O_9$	$C_{23}H_{15}CdN_2O_5$
M_r (g mol^{-1})	895.72	902.16	648.06	683.19	511.77
Space group	*P*-1	*P*-1	$P2_1/c$	*P*-1	*C*2/*c*
Crystal system	triclinic	triclinic	monoclinic	triclinic	monoclinic
a (Å)	11.074	11.101(5)	12.2315(11)	8.864	18.0556(16)
b (Å)	12.321	12.172(5)	16.6441(15)	11.707	18.7708(17)
c (Å)	16.639	16.902(6)	14.4828(14)	13.803	12.1154(11)
α (°)	72.99	70.943(7)	90	70.47	90
β (°)	76.2	73.284(7)	108.1674(18)	87.29	112.4252(16)
γ (°)	74.55	75.876(7)	90	77.10	90
V (Å^3)	2060.6	2038.9(14)	2801.5(4)	1315.2	3795.6(6)
Z	2	2	4	2	8
D_c (g/cm^3)	1.444	1.469	1.537	1.725	1.791
μ (mm^{-1})	0.488	0.675	0.840	1.889	1.192
R_{int}	0.0461	0.0572	0.0396	0.0179,	0.0256,
Limiting indices	$-13 \le h \le 13$ $-14 \le k \le 14$ $-17 \le l \le 19$	$-13 \le h \le 13$ $-14 \le k \le 14$ $-20 \le l \le 14$	$-14 \le h \le 12$ $-15 \le k \le 19$ $-13 \le l \le 17$	$-10 \le h \le 10$ $-13 \le k \le 7$ $-16 \le l \le 16$	$-15 \le h \le 21$ $-20 \le k \le 22$ $-13 \le l \le 14$
Reflns collected	10,672	10,244	14,210	6811	9666
Indep. reflns	7213	7128	4938	4613	3353
parameters	570	571	408	388	280
GOF on F^2	0.999	0.866	1.077	1.300	1.116
Final Rindices [$I>2\sigma(I)$]	$R_1 = 0.0665$, $wR_2 = 0.1621$	$R_1 = 0.0728$, $wR_2 = 0.1685$	$R_1 = 0.0391$, $wR_2 = 0.1022$	$R_1 = 0.0375$, $wR_2 = 0.1136$	$R_1 = 0.0914$, $wR_2 = 0.1718$
Rindices (all data)	$R_1 = 0.1345$, $wR_2 = 0.2166$	$R_1 = 0.1769$, $wR_2 = 0.2121$	$R_1 = 0.0577$, $wR_2 = 0.1096$	$R_1 = 0.0461$, $wR_2 = 0.1227$	$R_1 = 0.1164$, $wR_2 = 0.1837$

3.2. Structural description of coordination polymers 1-5

3.2.1. Crystal structures of 1 and 2

The single-crystal X-ray diffraction analysis reveal that **1** and **2** are isomorphous and isostructural, both **1** and **2** crystallize in triclinic with the space group *P*-1. Here, coordination polymer **1**, namely, $[Co(H_2ttac)(phen)_2]\cdot 4H_2O$, is selected as an example to describe the formation of its structure in detail. The coordination environment of Co(II) center is six-coordinated by two oxygen atoms from one deprotonated carboxyl belonging to one H_2ttac^{2-} ligand in chelating mode, together with four nitrogen atoms from two phen molecules to give a distorted $\{CoN_4O_2\}$ octahedral coordination geometry with the equatorial plane occupied by O1, O2, N1 and N4. The axial sites are occupied by N2 and N3 atoms (as shown in Fig. 1a). The H_2ttac^{2-} carboxylate anion displays μ_1-η^1:η^1 coordination mode (mode *a*, see Scheme 2). The Co–O distances range from 2.084(4)–2.203(3) Å, and those of Co–N are in the range of 2.092(5)–2.133(5) Å, respectively, which are consistent with those in previous work covering Co(II) coordination polymers [39–41].

The adjacent 0D discrete units are connected by two types strong noncovalent π–π stacking interactions involving the phenyl rings or the pyridine rings in phen ligands with the centroid-to-centroid distances of 3.5995 Å (between the parallel phenyl rings in phen) and 3.5690 Å (between the parallel pyridine rings in phen to construct a 1D infinite zigzagged chain (see Fig. 1b). The neighboring reciprocally parallel 1D chains are arranged into 2D sheet through C–H$\cdots\pi$ interactions (i.e. C5–H5$\cdots\pi$ = 3.1769 Å, π is defined by the phenyl ring in phen (C25–C26–C27–C28–C32–C33), as illustrated in Fig. 1c), which are further linked into a supramolecular 3D framework *via* π–π interactions between the parallel and partially overlapping phenyl rings of tetracarboxylic ligands with the vertical distance of 3.4981 Å (i.e. two rings are defined by the phenyl ring in tetracarboxylic as (C9–C10–C11–C12–C13–C14 and C9′–C10′–C11′–C12′–C13′–C14′), see Fig. 1d. Topologically, if the discrete motifs of $[Co(H_2ttac)(phen)_2]$ are viewed as nodes, the entire 3D structure can be simplified as shown in Fig. 1e.

3.2.2. Crystal structure of 3

Coordination polymer **3** crystallizes in the monoclinic with the space group $P2_1/c$. The Cu(II) center is coordinated by two carboxylate oxygen atoms from two partially deprotonated H_2ttac^{2-} ligands, two nitrogen atoms from one phen chelating

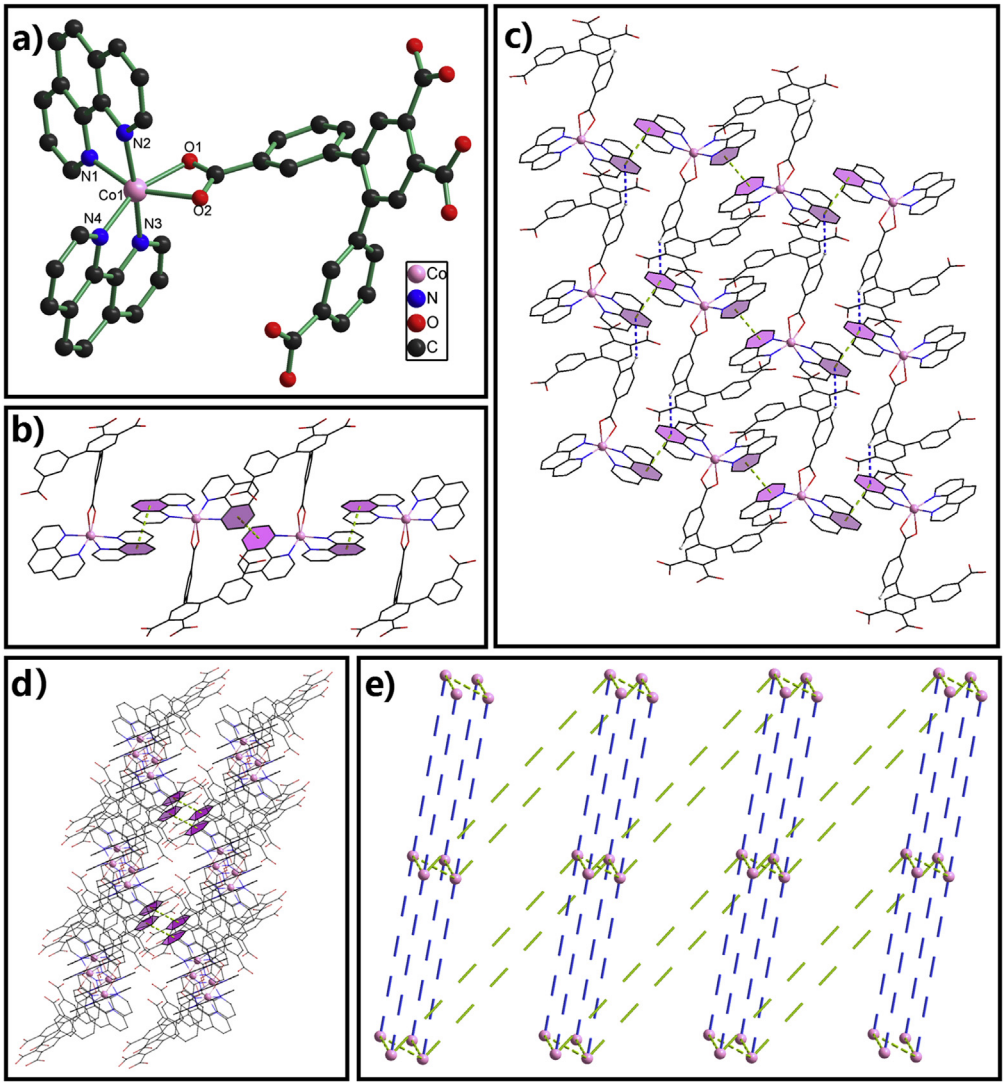

Fig. 1. (a) The coordination environment around Co(II) in **1** (H atoms are omitted for clarity). (b) The formation of 1D zigzagged chain through π–π stacking of adjacent 0D units. (c) The construction of 1D to 2D layer through C–H···π interaction. (d) View of 2D to 3D through π–π stacking. (e) The 3D topological structure.

ligand to form a four-coordinated $\{CuO_2N_2\}$ highly distorted quadrilateral configuration (see Fig. 2a). The bond lengths of Cu–N are in the range of 1.991(2)–2.002(2) Å and those of Cu–O are of 1.9414(17)–1.9250(19) Å. What is worth mentioning is that the single- and double-bond distances in the uncombined carboxylate groups [(1.207(3)–1.322(4) Å for O(3)–C(8), O(8)–C(16), O(4)–C(8) and O(7)–C(16)] of H_2ttac^{2-} ligand (see ESI CIF and Table S2) obviously show some differences between single- and double-bond character, while almost identical bond lengths in the coordinated carboxylate groups in **3** [1.239(3)–1.275(3) Å for O(2)–C(1), O(5)–C(15), O(1)–C(1) and O(6)–C(15)] are observed, consistent with delocalization as a result of the coordination of the carboxylate groups to Cu(II) [42–44].

Each H_2ttac^{2-} ligand links to two Cu(II) ions using its two carboxylate groups (i.e. O1–C1–O2 and O5–C15–O6), both of which adopt a monodentate coordination mode (mode *b*, μ_1-η^1:η^1, see Scheme 2) to join into a 1D infinite zigzagged chain along the *a* axis (see Fig. 2b), in which the phen ligands coordinate to the Cu(II) ions pointing away and being almost vertically from the *a* axis which may be beneficial to the formation of the π–π interactions later. The neighboring reciprocally parallel 1D chains are arranged into 2D sheet through π–π interactions between the parallel and partially overlapping the pyridine rings in phen and phenyl rings in H_2ttac^{2-} ligand with the vertical distance of 3.7858 Å (i.e. two rings are defined by the phenyl ring in phen as C23–C24–C25–C26–C27–N1 and C9–C10–C11–C12–C13–C14), see Fig. 2d. Nitrogen-containing in an aromatic ring may give rise to the differentiation of electron distributions, thus it may improve the stacking-type preferences and strengthen the π–π interactions. In the $\{CuO_2N_2\}$ distorted quadrilateral configuration, there are two uncoordinated carboxylic oxygen atoms presenting weak interaction with Cu(II) center at the axial site (Cu–O7 = 2.7665 Å and Cu–O4 = 2.6478 Å) due to the Jahn-Teller effect (see Fig. 2c), based on which to connect the adjacent layers into 3D architecture (see Fig. 2e). Topologically, if the discrete motifs of $[Co(H_2ttac^{2-})(phen)_2]$ are viewed as nodes, the entire 3D structure can be simplified as shown in Fig. 2f.

3.2.3. Crystal structure of 4

Coordination polymer **4** crystallizes in the triclinic system with the space group of *P*-1. The structure contains two crystallographically independent Zn(II) ions. As illustrated in Fig. 3a, Zn1 ion is four-coordinated and shows a similar distorted {ZnO4} tetrahedral geometry. The four oxygen atoms (O4, O6, O7 and O8) bonding with Zn1 come from four individual μ_6-η^1:η^1:η^1:η^1:η^1:η^1:η^1 (μ_6-$ttac^{4-}$) ligands (Scheme 2), while Zn2 ion is five-coordinated and exhibits a distorted {ZnN2O3} tetragonal pyramid configuration. Around Zn2 ion, the two nitrogen atoms (N1and N2) belong to dimidazole ligand, two oxygen atoms (O1 and O5) come from two individual μ_6-η^1:η^1:η^1:η^1:η^1:η^1:η^1 (μ_6-$ttac^{4-}$) ligands and one from one water molecule. Zn1 and Zn2 are bridged by one μ_6-η^1:η^1-carboxyl from H_2ttac^{2-} ligand with the distance of 4.2168(6) Å. In contrast to **1**, **2** and **3**, the carboxylic groups in the ligand in **4** are completely deprotonated and employ more complicated coordination mode (mode *c*, Scheme 2). The $ttac^{4-}$ anion acts as a μ_6-bridge connecting six Zn(II) ions, which is rarely observed in H_4ttac-based coordination polymers. The bond lengths of Zn–N (2.070(3)–2.157(3)Å), Zn–O (1.931(2)–2.017(2) Å) and Zn–OW (2.153(3) Å) in **4** are in good agreement with the literature values [45–48].

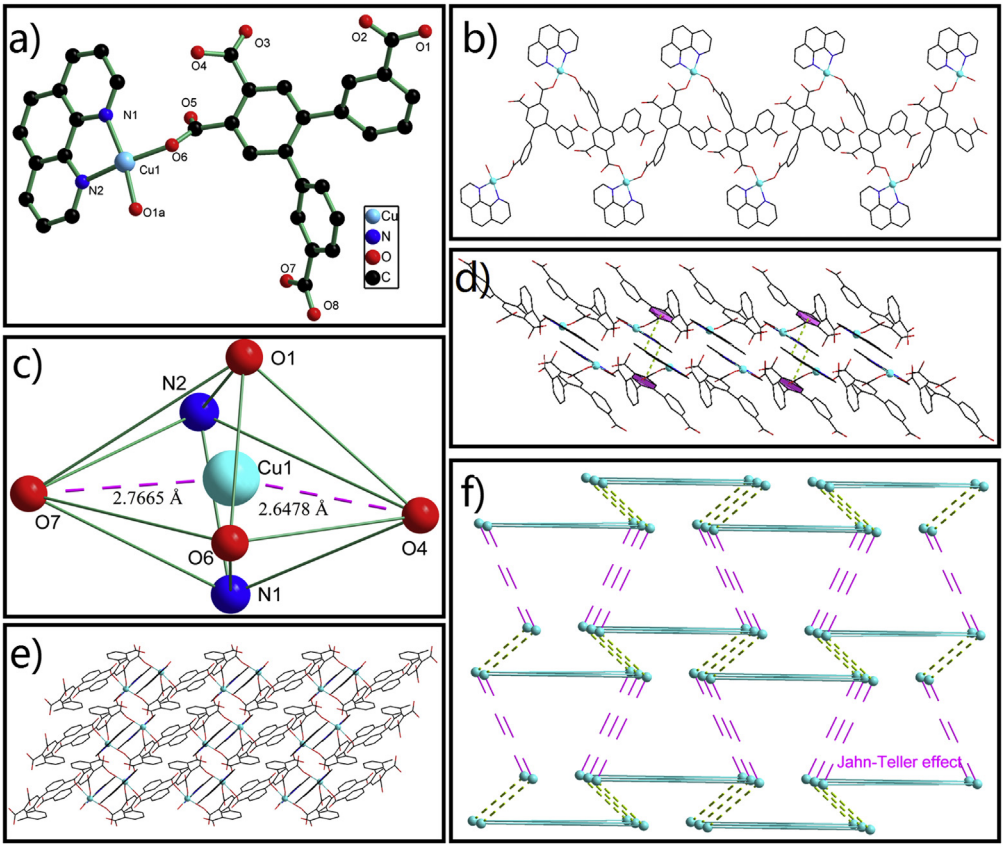

Fig. 2. (a) The coordination environment around Cu(II) in **3** (H atoms are omitted for clarity). (b) The 1D zigzagged chain. (c) The Jahn-Teller effect in coordination polymer **3**. (d) The construction of 1D to 2D layer through π–π stacking. (e) The 3D architecture of coordination polymer **3**. (f) The 3D topological structure.

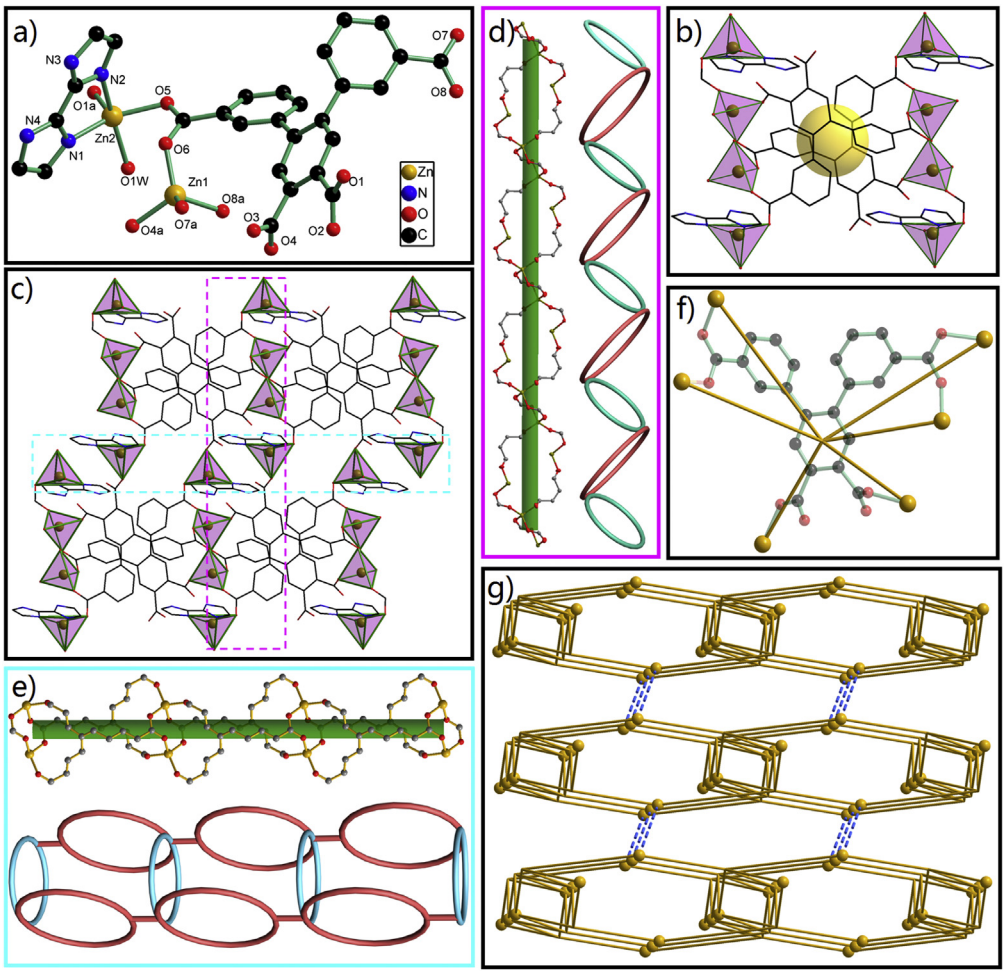

Fig. 3. (a) The coordination environments around Zn(II) centers in **4** (H atoms are omitted for clarity). (b) The SBUs of coordination polymer in **4**. (c) The 2D layer in coordination polymer **4**. (d) and (e) Two types of hollow channel in the 2D layer. (f) The simple mode of topological graph. (g) The 3D topological structure of **4**.

As shown in Fig. 3b, every two hexadentate ttac^{4-} ligands connect eight Zn(II) ions to form a closed-ring-like motif, based on which to fabricate into a 2D double-layered network (see Fig. 3c). One architectural feature particularly worth mentioning is that two types of hollow channel are observed in the 2D layer and each of which may allow one virtual cylinder to penetrate through, respectively, as illustrated in Fig. 3d and e. From the topological point of view, all ttac^{4-} ligands can be regarded as 6-connected nodes, and the 2D layer may be topologically simplified as the architecture as shown in Fig. 3f. In the crystal structure, the adjacent 2D layers are linked by C–H$\cdots\pi$ (i.e. C11–H11$\cdots\pi$ = 2.9250 Å, as signified in the blue(in the web version) dashed line in Fig. 3g) interactions to generate a final 3D metal-organic framework.

3.2.4. *Crystal structure of 5*

Coordination polymer **5** crystallizes in the monoclinic system with the space group of *C* 2/*c*. Cd(II) center exhibits a distorted {CdN2O4} octahedral geometry that is completed with one oxygen atom of one ttac^{4-} (O1), two nitrogen atoms (N1and N2) from one molecule of phen, and one terminal H_2O molecule (O1W) at the equatorial plane, as well as another two carboxylate oxygen atoms belong to the other two ttac^{4-} ligands occupying the axial site (O2a and O3a, see Fig. 4a). The bond lengths of the Cd–N vary from 2.327(8) to 2.388(8) Å, the Cd–O bond distances range from 2.305(7) to 2.524(10) Å, and that of Cd–OW is 2.208(10) Å, which are all in the normal ranges [49–52].

The carboxylic groups in the ligand in **5** are completely deprotonated and employ more complicated μ_6-η^1:η^1:η^1:η^1:η^1:η^1:η^1 (μ_6-ttac^{4-}) coordination mode (mode *d*, Scheme 2). The octahedral Cd(II) centers in **5** are aggregated to the {Cd4(O–C–O)4} clusters by the carboxylate groups of ttac^{4-} ligands. Interconnected by the building block of {Cd4(O–C–O)4} clusters and the 6-connected node of μ_6-ttac^{4-} ligands (Fig. 4d), **5** is manufactured into a 2D layer which is further concatenated into a 3D metal-organic framework through μ_6-ttac^{4-} ligands, as illustrated in Fig. 4b and c. In the other aspect, the assembling of 3D metal-organic framework of **5** may also be interpreted as being interconnected *via* the parallel zigzagged 1D chains (see Fig. 4e and f). The entire 3D topological structure can be simplified as shown in Fig. 4g.

3.3. *Magnetic properties*

As well as we known, the magnetic properties of coordination polymers have generally been well explored. The majority of magnetic coordination polymers contain paramagnetic metal centres (V, Cr, Mn, Fe, Co, Ni and Cu), which illustrate the potential of producing magnets because of the first row transition metals may exist in different oxidation states and allow variation of the two

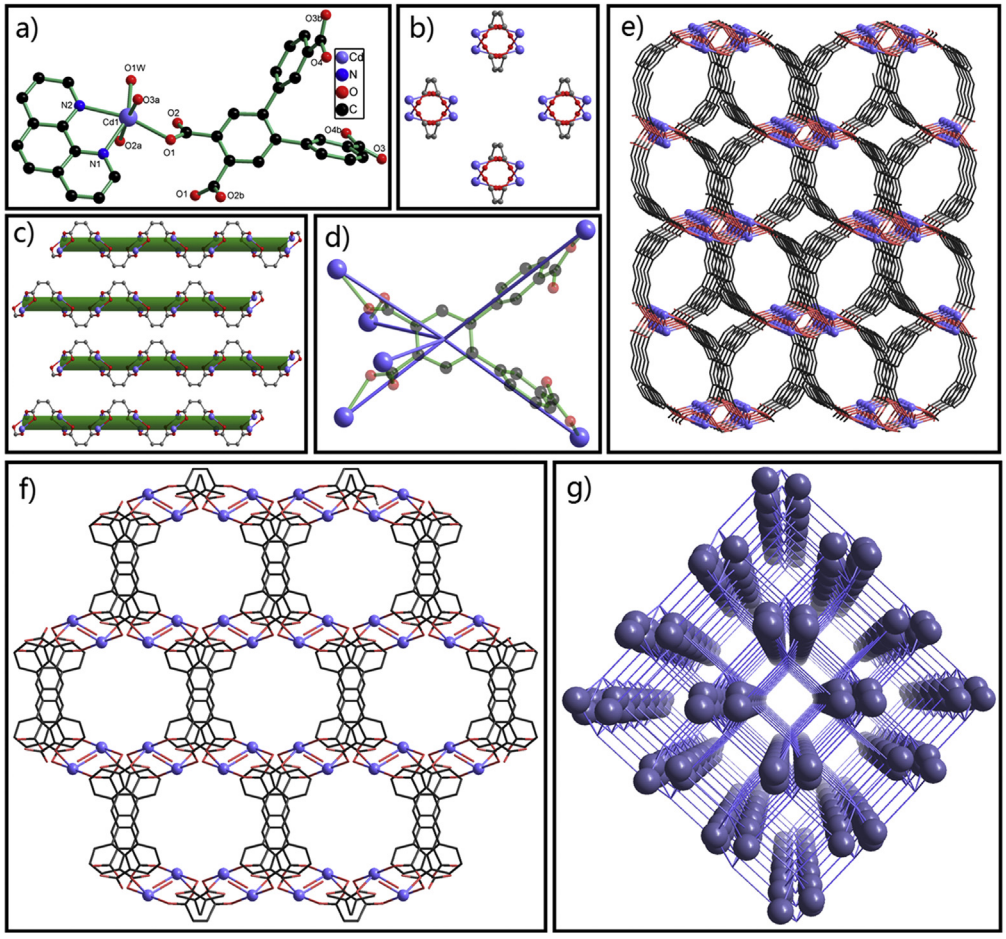

Fig. 4. (a) The coordination environment around Cd(II) in **5** (H atoms are omitted for clarity). (b) and (c) The 1D zigzagged chains viewed along different directions. (d) The simple mode of topological graph. (e) and (f) The 3D network viewed along different directions. (g) The topological graph of coordination polymer **5** showing the 3D architecture connected through ttac4-linkers among the adjacent 1D chains.

important parameters, spin quantum number and magnetic anisotropy [44,53–58].

The coordination polymer **3** has a chain structure with Cu(II) centers and may be a single-chain magnet. Variable-temperature magnetic susceptibility of **3** is measured in the temperature range of 2.0–300.0 K. The variation of the inverse magnetic susceptibility χ_M^{-1} and $\chi_M T$ of **3** with temperature is shown in Fig. 5. The thermal evolution of χ_M^{-1} obeys the Curie–Weiss law; namely, $\chi_M = C/(T-\theta)$ in the range of 2.0–300.0 K, and Weiss constant θ and Curie constant C_M are −2.240 K and 0.425 $cm^3\,K\cdot mol^{-1}$, respectively. The $\chi_M T$ value at 300.0 K is 0.425 $cm^3\,K\cdot mol^{-1}$ (1.843 μ_B), and it is little lower than the expected value (0.433 $cm^3\,K\cdot mol^{-1}$, 1.862 μ_B) for magnetically 1D chain Cu(II)($S_{Cu} = 1/2$, $g = 2.15$). Besides, the $\chi_M T$ value of **3** tends to decrease with declining temperature and it reaches a minimum of 0.385 $cm^3\,K\cdot mol^{-1}$ at 3.8 K. The negative θ value and the $\chi_M T$ *vs.* *T* curve of coordination polymer **3** reveals typical antiferromagnetic interactions between the Cu(II) centers. Moreover, the distances of Cu···Cu is 14.0901(11) Å, which suggests that the observed antiferromagnetic interaction of **3** should arise from the magnetic super exchange through the $(O_2C\text{-}Ar\text{-}Ar\text{-}CO_2)_2$ bridges.

3.4. Thermal analysis

The thermal analysis of coordination polymers **3** and **4** have been measured from 25 to 1000 °C with a heating rate of 10 °C min^{-1} in N_2 flow (Fig. S2). For coordination polymer **3**, there is no strictly clean weight loss step occurred below 265 °C and the framework collapse a sharp decomposition take place (weight loss of 77.70%) from 265 to 500 °C, which can be assigned to the loss of $ttac^-$ and phen (theoretical loss 87.72%). The remnant of coordination polymer **3** is CuO 16.51% (theoretical value 12.28%) which

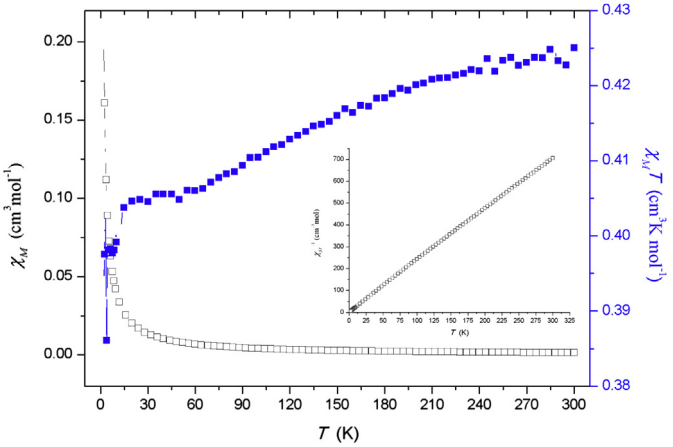

Fig. 5. Thermal variation of χ_M and $\chi_M T$ for coordination polymer **3**. Insert: Plot of thermal variation of χ_M^{-1} for coordination polymer **3**.

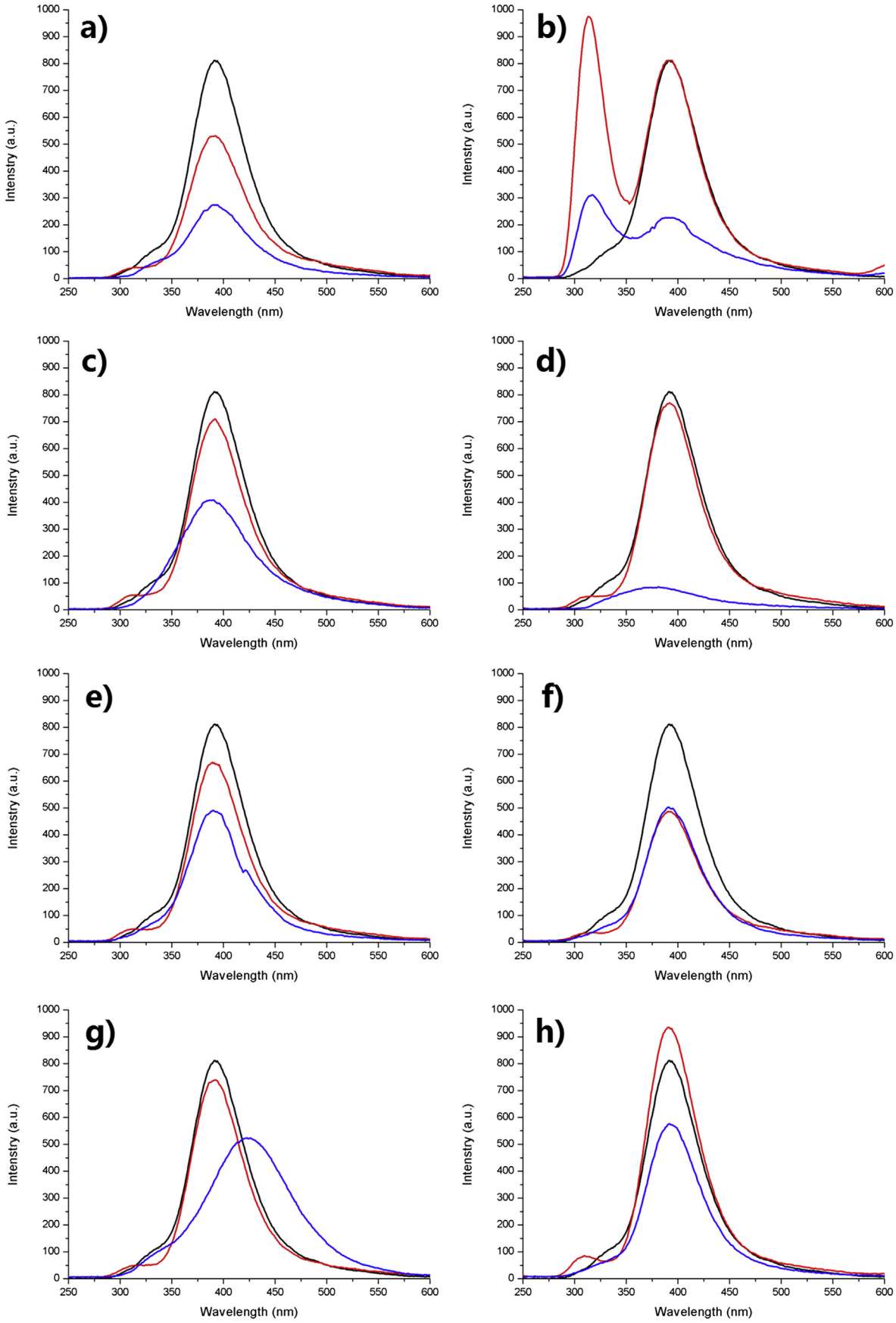

Fig. 6. The emission spectra of the coordination polymer **3** and amino acids at room temperature (Black, coordination polymer **3**; Red, amino acids; Blue, mixture of coordination polymer **3** and amino acids). (a) L-Threonine, (b) L-Tyrosine, (c) L-Glutamate, (d) L-Arginin, (e) L-Histidine, (f) L-Glutamine, (g)L-(h) Cysteine and (h) L-Phenylalanine. (For interpretation of the references to color in this figure legend, the reader is referred to the web version of this article.).

suggests that it does not decompose completely under the experimental temperature. For coordination polymer **4**, the first weight loss stage has a decomposition temperature range of 25–125 °C, with a weight loss of 2.43% (theoretical loss 2.64%), which can likewise be assigned to the loss of one molecules H_2O. The second stage weight loss (75.31%) of 390–1000 °C owing to the ligands decomposition and conforming to the loss of single H_4ttac and DMZ (theoretical loss 73.53%). The remnants of coordination polymers **4** is 22.03% consistent with the crystal structure analysis (theoretical value 23.83%). The thermal analysis (TG) measurement showed good thermal stability because of coordination polymers **3** (before 265 °C) and **4** (before 390 °C) have intact structure.

3.5. Luminescent properties

From a fundamental point of view, the ordered nature of coordination polymers structures suggests their use as a platform for research on energy transfer. The linker-based luminescence includes ligand-localized emission ligand-to-metal charge transfer (LMCT) and metal-to-ligand charge transfer (MLCT). Although luminescent coordination polymers have yet to be incorporated into actual sensing devices, several recent reports illustrate their have been investigated for the fabrication of different chemical sensors. The various luminescent properties of coordination polymers would to make them ideal for molecular recognition [4,59–66].

To examine the possibility of adjusting of the luminescent properties through amino acids exchange, the solid sample of coordination polymer **3** was immersed in water (10^{-4} M) containing various amino acids to generate solutions at room temperature. The emission spectra (392 nm) of the coordination polymer in the presence of L-Threonine (a), L-Tyrosine (b), L-Glutamate (c), L-Arginin (d), L-Histidine (e), L-Glutamine (f), L-Cysteine (g) and L-Phenylalanine (h) with respect to the coordination polymer are graphically expressed in Fig. 6 and Fig. 7, respectively. Detailedly, in the presence of L-Arginin, the emission intensity of **3** at 392 nm (excited at 241 nm) is declined sharply by more than 10 times (from 811 to 78 a.u.). Furthermore, blue shift occurs in the emission spectrum of **3** (from 392 to 375 nm), see Fig. 6d. The high selectivity for L-Arginin sensing probably results from the electrostatic interaction between $-COO^-$ anions (deriving from the free carboxyl groups of side chains in the polymeric backbone) and $-NH_3^+$ cations (belonging to amino acids), which affords signal amplification [67,68]. In another aspect, the weaken luminescent intensities of **3** in aqueous solution may be mainly caused by effective intramolecular energy transfer from the H_2ttac^{2-} ligands to the central Cu(II)(LMCT), and this energy transfer process may be triggered to a significant decrease of its fluorescent intensity in aqueous solution by the introduction of preferring configurations of amino acids, such as Arginin in this case. To further elucidate the possible recognition mechanism of **3** towards L-Arginin, we have made efforts to obtain single crystal of L-Arginin connected with **3** in water but without success so far.

Similar experiment shows that the introduction of L-Cysteine leads to slightly decrease of the emission intensity of **3** (from 811 to 537 a.u.). Meanwhile, red shift in the emission spectrum of **3** is observed (from 392 to 425 nm), see spectrum Fig. 6g.

As far as the other tested amino acids are concerned, as compared with coordination polymer **3**, the corresponding amino acids in the aqueous solutions exhibits emission bands with unchanged position and slightly changed intensity (excited at 241 nm). Thus it can be seen that, coordination polymer **3** shows high selectivity of L-Arginin over other amino acids.

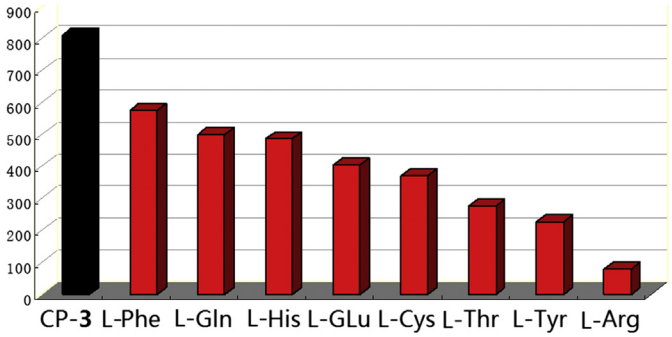

Fig. 7. The luminescent intensities of the coordination polymer **3** upon the addition of various amino acids at room temperature (excited at 241 nm).

4. Conclusion

In summary, we have successfully synthesized a series of coordination polymers with flexible H_4ttac ligand and nitrogen-containing auxiliary ligands. Structural analysis reveals that the as-synthesized coordination polymers present different structures, ranging from zero-, one-, two-to three-dimensions, which are mainly due to the different metal ions, the degree of deprotonation and coordination modes of the H_4ttac ligand. Based on the diversified $\pi-\pi$ stacking (phenyl–phenyl, phenyl–pyridine, pyridine–pyridine $\pi-\pi$ interactions) and/or C–H$\cdots\pi$ interactions between corresponding aromatic rings of H_4ttac ligands and/or nitrogen-containing auxiliary ligands, **1**–**4** are finally generated form low-dimensional structures into three-dimensional frameworks, suggesting that utilizing these intermolecular forces are of effective strategies in the assembly of the high-dimensional coordination polymers, especially when strong hydrogen bonds are absent. In the three types $\pi-\pi$ stacking interactions, nitrogen-containing in the aromatic rings may show preferences of crystal structures with stacking owing to the differentiation of π (and σ) electron distributions caused by heteroatoms in an aromatic system. Experiments proved that coordination polymer **3** displays antiferromagnetic property and selective recognition towards L-Arginin which may be a promising fluorescent probe of L-Arginin. This investigation may provide new insight into the field of precisely controlling the interaction among targeting amino acids with recognition precursors (such as metal coordination polymers) and potential applications in chemo- and biosensing. In this work, H_4ttac ligand presents a good candidate in the assembly of coordination polymers due to its diversities and flexibility of coordination modes. The systematic investigations on the coordination modes of H_4ttac ligand together with the nitrogen-containing auxiliary ligands may achieve new expectations to fabricate new coordination polymers with multifunctionalities, such as magnetism and fluorescence properties which are our ongoing work recently.

Acknowledgments

This research is financially supported by the Natural Science Foundation of Henan Province of China (Nos.13A150056, and 15NB005).

Appendix A. Supplementary data

Supplementary data related to this article can be found at http://dx.doi.org/10.1016/j.dyepig.2015.06.035.

References

[1] Zhao X, Xiao B, Fletcher AJ, Thomas KM, Bradshaw D, Rosseinsky MJ. Hysteretic adsorption and desorption of hydrogen by nanoporous metal-organic frameworks. Science 2004;306(5698):1012–5.

[2] Li L, Tang S, Wang C, Lv X, Jiang M, Wu H, et al. High gas storage capacities and stepwise adsorption in a UiO type metal-organic framework incorporating Lewis basic bipyridyl sites. Chem Commun 2014;50(18):2304–7.

[3] Chen B, Wang L, Xiao Y, Fronczek FR, Xue M, Cui Y, et al. A luminescent metal-organic framework with Lewis basic pyridyl sites for the sensing of metal ions. Angew Chem Int Ed 2009;48(3):500–3.

[4] Chen B, Yang Y, Zapata F, Lin G, Qian G, Lobkovsky EB. Luminescent open metal sites within a metal-organic framework for sensing small molecules. Adv Mater 2007;19(13):1693–6.

[5] Zhu QL, Xu Q. Metal-organic framework composite. Chem Soc Rev 2014;43(16):5468–512.

[6] Ke F, Yuan YP, Qiu LG, Shen YH, Xie AJ, Zhu JF, et al. Facile fabrication of magnetic metal-organic framework nanocomposites for potential targeted drug delivery. J Mater Chem 2011;21(11):3843–8.

[7] Wang B, Côté AP, Furukawa H, O'Keeffe M, Yaghi OM. Colossal cages in zeolitic imidazolate frameworks as selective carbon dioxide reservoirs. Nature 2008;453(7192):207–11.

[8] Lin ZJ, Lü J, Hong M, Cao R. Metal-organic frameworks based on flexible ligands (FL-MOFs): structures and applications. Chem Soc Rev 2014;43(16):5867–95.

[9] Gao WY, Zhang Z, Cash L, Wojtas L, Chen YS, Ma S. Two rare indium-based porous metal-metalloporphyrin frameworks exhibiting interesting CO_2 uptake. CrystEngComm 2013;15(45):9320–3.

[10] Serra-Crespo P, Dikhtiarenko A, Stavitski E, Juan-Alcañiz J, Kapteijn F, Coudert FX, et al. Experimental evidence of negative linear compressibility in the MIL-53 metal-organic framework family. CrystEngComm 2015;17(2):276–80.

[11] Lu Z, Du L, Zheng B, Bai J, Zhang M, Yun R. A highly porous agw-type metal-organic framework and its CO_2 and H_2 adsorption capacity. CrystEngComm 2013;15(45):9348–51.

[12] Deng H, Doonan CJ, Furukawa H, Ferreira RB, Towne J, Knobler CB, et al. Multiple functional groups of varying ratios in metal-organic frameworks. Science 2010;327(5967):846–50.

[13] He Y, Li B, O'Keeffe M, Chen B. Multifunctional metal-organic frameworks constructed from meta-benzenedicarboxylate units. Chem Soc Rev 2014;43(16):5618–56.

[14] Basdogan Y, Keskin S. Simulation and modelling of MOFs for hydrogen storage. CrystEngComm 2015;17:261–75.

[15] Halder GJ, Kepert CJ, Moubaraki B, Murray KS, Cashion JD. Guest-dependent spin crossover in a nanoporous molecular framework material. Science 2002;298(5599):1762–5.

[16] Roy B, Mukherjee S, Mukherjee PS. Sr^{2+} and Cd^{2+} coordination polymers: the effect of the different coordinating behaviour of a newly designed tricarboxylic acid. CrystEngComm 2013;15(45):9596–602.

[17] Chen JX, Chen M, Ding NN, Chen WH, Zhang WH, Hor TA, et al. Transmetalation of a dodecahedral Na9 aggregate-based polymer: a facile route to water stable Cu(II) coordination networks. Inorg Chem 2014;53(14):7446–54.

[18] Li L, Bell JG, Tang S, Lv X, Wang C, Xing Y, et al. Gas storage and diffusion through nanocages and windows in porous metal-organic framework Cu_2(2,3,5,6- tetramethylbenzene-1,4-diisophthalate)$(H_2O)_2$. Chem Mater 2014;26(16):4679–95.

[19] Bureekaew, Balwani V, Amirjalayer S, Schmid R. Isoreticular isomerism in 4, 4-connected paddle-wheel metal-organic frameworks: structural prediction by the reverse topological approach. CrystEngComm 2015;17(2):344–52.

[20] Yang LR, Wu LZ, Liu L, Zhang HM, Li MX. Three novel transition metal coordination polymers based on (2,3-f)-pyrazino(1,10) phenanthroline-2,3-dicarboxylic acid sodium salt: hydrothermal syntheses, structures, and properties. Dyes Pigm 2014;2(101):196–202.

[21] Xue YS, He Y, Zhou L, Chen FJ, Xu Y, Du HB, et al. A photoluminescent microporous metal organic anionic framework for nitroaromatic explosive sensing. J Mater Chem A 2013;1(14):4525–30.

[22] Guillerm V, Weseliński ŁJ, Belmabkhout Y, Cairns AJ, D'Elia V, Wojtas Ł, et al. Discovery and introduction of a (3,18)-connected net as an ideal blueprint for the design of metal-organic frameworks. Nat Chem 2014;6:673–80.

[23] Peikert K, Hoffmann F, Fröba M. Fluorine magic: one new organofluorine linker leads to three new metal–organic frameworks. CrystEngComm 2015;17(2):353–60.

[24] Muche S, Levacheva I, Samsonova O, Pham L, Christou G, Bakowsky U, et al. A chiral, low-cytotoxic $[Ni_{15}]$-wheel complex. Inorg Chem 2014;53(14):7642–9.

[25] Lv X, Li L, Tang S, Wang C, Zhao X. High CO_2/N_2 and CO_2/CH_4 selectivity in a chiral metal-organic framework with contracted pores and multiple functionalities. Chem Commun 2014;50(52):6886–9.

[26] Li YW, Hu TL, Liu SJ, Bu XH. Doping cobalt into a $[Zn_7]$ cluster-based MOF to tune magnetic behaviour and induce fluorescence signal mutation. Dalton Trans 2014;43(30):11470–3.

[27] Dias SS, André V, Kłak J, Duarte MT, Kirillov AM. Topological diversity of supramolecular networks constructed from copper(II) aminoalcohol blocks and 2, 6-naphthalenedicarboxylate linkers: self-assembly synthesis, structural features, and magnetic properties. Cryst Growth Des 2014;14(7):3398–407.

[28] Liang G, Liu Y, Zhang X, Yi Z. Anion-dependent assemblies of a series of Cd (ii) coordination complexes based on an asymmetric multi-dentate ligand and inorganic SBUs: syntheses, crystal structures, and fluorescent properties. CrystEngComm 2014;16(42):9896–906.

[29] Li YM, Lun HJ, Xiao CY, Xu YQ, Wu L, Yang JH, et al. A bilayer triangular lattice with crown-like Co_7 spin cluster SBUs exhibiting high spin frustration. Chem Commun 2014;50(62):8558–60.

[30] Dau PV, Cohen SM. The influence of nitro groups on the topology and gas sorption property of extended Zn(II)-paddlewheel MOFs. CrystEngComm 2013;15(45):9304–7.

[31] Hu FL, Yi M, Gu YQ, Zhu LG, Yang SL, Wei H, et al. Structure diversities of ten entangled coordination polymers assembled from reactions of Co(II) or Ni(II) salts with 5-(pyridin-4-yl) isophthalic acid in the absence or presence of auxiliary N-donor ligands. CrystEngComm 2013;15(45):9553–61.

[32] Sen S, Neogi S, Aijaz A, Xu Q, Bharadwaj PK. Construction of non-interpenetrated charged metal-organic frameworks with doubly pillared layers: pore modification and selective gas adsorption. Inorg Chem 2014;53(14):7591–8.

[33] Li Q, Qian J. Multifarious zinc coordination polymers based on biphenyl-3,3′,5,5′-tetracarboxylate and different flexibility of N-donor ligands. RSC Adv 2014;4(61):32391–7.

[34] Wang F, Jing X, Zheng B, Li G, Zeng G, Huo Q, et al. Four Cd-based metal-organic frameworks with structural varieties derived from the replacement of organic linkers. Cryst Growth Des 2013;13(8):3522–7.

[35] Jia C, Lin Q, Yuan W. A series of coordination polymers constructed by a flexible tetracarboxylic acid: synthesis, structural diversity and luminescent properties. CrystEngComm 2014;16(12):2508–19.

[36] Główka ML, Martynowski D, Kozłowska K. Stacking of six-membered aromatic rings in crystals. J Mol Struct 1999;474(1):81–9.

[37] Reger DL, Horger JJ, Smith MD, Long GJ, Grandjean F. Homochiral, helical supramolecular metal-organic frameworks organized by strong $\pi\cdots\pi$ stacking interactions: single-crystal to single-crystal transformations in closely packed solids. Inorg Chem 2010;50(2):686–704.

[38] Janiak C. A critical account on $\pi-\pi$ stacking in metal complexes with aromatic nitrogen-containing ligands. J Chem Soc Dalton Trans 2000;21:3885–96.

[39] Uemura K, Kitagawa S, Kondo M, Fukui K, Kitaura R, Chang HC, et al. Novel flexible frameworks of porous Cobalt(II) coordination polymers that show selective Guest adsorption based on the switching of hydrogen-bond pairs of Amide groups. Chem Eur J 2002;8(16):3586–600.

[40] Li JR, Yu Q, Tao Y, Bu XH, Ribas J, Batten SR. Magnetic canting or not? Two isomorphous 3D Co^{II} and Ni^{II} coordination polymers with the rare non-interpenetrated (10,3)-d topological network, showing spin-canted antiferromagnetism only in the Co^{II} system. Chem Commun 2007;43(22):2290–2.

[41] Ma LF, Wang LY, Wang YY, Batten SR, Wang JG. Self-assembly of a series of cobalt (II) coordination polymers constructed from H_2tbip and dipyridyl-based ligands. Inorg Chem 2008;48(3):915–24.

[42] Sun YG, Gu XF, Ding F, Smet PF, Gao EJ, Poelman D, et al. Synthesis, crystal structures, and properties of novel heterometallic La/Pr–Cu–K and Sm/Eu/Tb–Cu coordination polymers. Cryst Growth Des 2010;10(3):1059–67.

[43] Park TH, Cychosz KA, Wong-Foy AG, Dailly A, Matzger AJ. Gas and liquid phase adsorption in isostructural Cu_3 [biaryltricarboxylate]$_2$ microporous coordination polymers. Chem Commun 2011;47(5):1452–4.

[44] Kathalikkattil AC, Bisht KK, Aliaga-Alcalde N, Suresh E. Synthesis, magnetic properties, and structural investigation of mixed-ligand Cu(II) helical coordination polymers with an amino acid backbone and N-donor propping: 1-D helical, 2-D hexagonal net (hcb), and 3-D ins topologies. Cryst Growth Des 2011;11(5):1631–41.

[45] Meng X, Song Y, Hou H, Fan Y, Li G, Zhu Y. Novel Pb and Zn coordination polymers: synthesis, molecular structures, and third-order nonlinear optical properties. Inorg Chem 2003;42(4):1306–15.

[46] Lu WG, Jiang L, Feng XL, Lu TB. Three 3D coordination polymers constructed by Cd(II) and Zn(II) with imidazole-4, 5-dicarboxylate and 4, 4'-bipyridyl building blocks. Cryst Growth Des 2006;6(2):564–71.

[47] Zheng SL, Chen XM. Recent advances in luminescent monomeric, multinuclear, and polymeric Zn(II) and Cd(II) coordination complexes. Aust J Chem 2004;57(8):703–12.

[48] Tian Z, Lin J, Su Y, Wen L, Liu Y, Zhu H, et al. Flexible ligand, structural, and topological diversity: isomerism in $Zn(NO_3)_2$ coordination polymers. Cryst Growth Des 2007;7(9):1863–7.

[49] Jin S, Wang D, Chen W. Synthesis, luminescence, and structural characterization of Zn and Cd coordination polymers of flexible bis (imidazolyl) derivatives. Inorg Chem Commun 2007;10(6):685–9.

[50] Meng X, Song Y, Hou H, Han H, Xiao B, Fan Y, et al. Hydrothermal syntheses, crystal structures, and characteristics of a series of Cd-btx coordination polymers (btx=1,4-bis (triazol-1-ylmethyl) benzene). Inorg Chem 2004;43(11):3528–36.

[51] Chen J, Li CP, Du M. Substituent effect of R-isophthalates (R= –H, $-CH_3$, $-OCH_3$, –tBu, –OH, and $-NO_2$) on the construction of Cd^{II} coordination polymers incorporating a dipyridyl tecton 2,5-bis(3-pyridyl)-1,3,4-oxadiazole. CrystEngComm 2011;13(6):1885–93.

[52] Li L, Wang S, Chen T, Sun Z, Luo J, Hong M. Solvent-dependent formation of Cd (II) coordination polymers based on a C_2-symmetric Tricarboxylate linker. Cryst Growth Des 2012;12(8):4109–15.
[53] Liang Y, Cao R, Su W, Hong M, Zhang W. Syntheses, structures, and magnetic properties of two gadolinium (III)–copper(II) coordination polymers by a hydrothermal reaction. Angew Chem Int Ed 2000;39(18):3304–7.
[54] Liang Y, Hong M, Su W, Cao R, Zhang W. Preparations, structures, and magnetic properties of a series of novel copper (II)-lanthanide(III) coordination polymers via hydrothermal reaction. Inorg Chem 2001;40(18):4574–82.
[55] Zheng YQ, Lin JL, Kong ZP. Coordination polymers based on Cobridging of rigid and flexible spacer ligands: syntheses, crystal structures, and magnetic properties of $[Mn(bpy)(H_2O)(C_4H_4O_4)]$ 0.5bpy, Mn $(bpy)(C_5H_6O_4)$, and Mn $(bpy)(C_6H_8O_4)$. Inorg Chem 2004;43(8):2590–6.
[56] Li DS, Zhao J, Wu YP, Liu B, Bai L, Zou K, et al. Co_5/Co_8–cluster-based coordination polymers showing high-connected self-penetrating networks: syntheses, crystal structures, and magnetic properties. Inorg Chem 2013;52(14):8091–8.
[57] Huang FP, Tian JL, Gu W, Liu X, Yan SP, Liao DZ, et al. Co(II) coordination polymers: positional isomeric effect, structural and magnetic diversification. Cryst Growth Des 2010;10(3):1145–54.
[58] Yuan G, Shan W, Liu B, Rong L, Zhang L, Zhang H, et al. Three Mn(II) coordination polymers with a bispyridyl-based quinolinate ligand: the anion-controlled tunable structural and magnetic properties. Dalton Trans 2014;43(25):9777–85.
[59] Bauer CA, Timofeeva TV, Settersten TB, Patterson BD, Liu VH, Simmons BA, et al. Influence of connectivity and porosity on ligand-based luminescence in zinc metal-organic frameworks. J Am Chem Soc 2007;129(22):7136–44.
[60] Lee EY, Jang SY, Suh MP. Multifunctionality and crystal dynamics of a highly stable, porous metal-organic framework $[Zn_4O(NTB)_2]$. J Am Chem Soc 2005;127(17):6374–81.
[61] Bai Y, He GJ, Zhao YG, Duan CY, Dang DB, Meng QJ. Porous material for absorption and luminescent detection of aromatic molecules in water. Chem Commun 2006;42(14):1530–2.
[62] Harbuzaru BV, Corma A, Rey F, Atienzar P, Jorda JL, Garcia H, et al. Metal–organic nanoporous structures with anisotropic photoluminescence and magnetic properties and their use as sensors. Angew Chem Int Ed 2008;47(6):1080–3.
[63] Qiu Y, Liu Z, Li Y, Deng H, Zeng R, Zeller M. Reversible anion exchange and sensing in large porous materials built from 4, 4′-bipyridine via $\pi\cdots\pi$ and H-bonding interactions. Inorg Chem 2008;47(12):5122–8.
[64] Dou Z, Yu J, Cui Y, Yang Y, Wang Z, Yang D, et al. Luminescent metal-organic framework films As highly sensitive and fast-response oxygen sensors. J Am Chem Soc 2014;136(15):5527–30.
[65] Li YW, Li JR, Wang LF, Zhou BY, Chen Q, Bu XH. Microporous metal-organic frameworks with open metal sites as sorbents for selective gas adsorption and fluorescence sensors for metal ions. J Mater Chem A 2013;1(3):495–9.
[66] Lei J, Qian R, Ling P, Cui L, Ju H. Design and sensing applications of metal-organic framework composites. TrAC Trends Anal Chem 2014;58:71–8.
[67] Zhou Y, Yoon J. Recent progress in fluorescent and colorimetric chemosensors for detection of amino acids. Chem Soc Rev 2012;41(1):52–67.
[68] Li H, Feng X, Guo Y, Chen D, Li R, Ren X, et al. A malonitrile-functionalized metal-organic framework for hydrogen sulfide detection and selective amino acid molecular recognition. Sci Rep 2014;4(4366):1–5.